Draft version February 15, 2010
Preprint typeset using LaTeX style emulateapj v. 11/10/09

MODELING BROADBAND X-RAY ABSORPTION OF MASSIVE STAR WINDS

Maurice A. Leutenegger[1,2], David H. Cohen[3], Janos Zsargó[4,5], Erin M. Martell[6,3], James P. MacArthur[3], Stanley P. Owocki[7], Marc Gagné[8], D. John Hillier[5]

Draft version February 15, 2010

ABSTRACT

We present a calculation of the transmission of X-rays in a spherically symmetric, partially optically thick stellar wind which can be used to model the broad-band soft X-ray emission due to shock-heated plasma distributed throughout a massive star's wind. We find the transmission by an exact integration of the formal solution, assuming the emitting plasma and absorbing plasma are mixed at a constant density ratio above some minimum radius, below which there is assumed to be no emission. This model is more realistic than either the slab absorption associated with a corona at the base of the wind or the exospheric approximation that assumes all the emission arises at and above the radius of optical depth unity. Our model is implemented in XSPEC as a pre-calculated table which can be coupled to a detailed table of the wavelength dependent wind opacity. Preliminary modeling of *Chandra* grating data indicates that the X-ray hardness trend of OB stars with spectral subtype can largely be understood as a wind absorption effect.

Subject headings: stars: early type — stars: winds, outflows — stars: mass-loss — techniques: spectroscopic

1. INTRODUCTION

The absorption of soft X-rays by the powerful, radiation-driven winds of OB stars has long been recognized as a significant effect both on the X-rays observed from these stars and on the physical conditions in their winds (Cassinelli & Olson 1979; Cassinelli & Swank 1983; Hillier et al. 1993; MacFarlane et al. 1994). The significant soft X-ray emission observed in OB stars by *Einstein* and *ROSAT* implied only modest wind attenuation of the X-rays, and thus ruled out significant coronal emission as a source of the ubiquitous X-ray emission seen in these massive stars. For this and other reasons, wind-shock models for the production of X-rays in OB stars have become accepted (e.g., Kahn et al. 2001), although many aspects of these models are still poorly understood.

Modeling not only the X-ray emission from OB star winds but also the absorption is crucial for advancing our understanding of the X-ray production mechanisms themselves. The amount and wavelength dependence of the wind absorption can be used as a diagnostic of the location/distribution of the shock-heated plasma, especially in terms of its effect on individual line profile shapes (Owocki & Cohen 2001, hereafter OC01). Even simply deriving an intrinsic X-ray luminosity for energy budget considerations requires correctly modeling the significant attenuation of the emitting X-rays, especially in the dense winds of O supergiants (Hillier et al. 1993; Owocki & Cohen 1999).

Because the emitting plasma is spatially distributed throughout the wind, simple prescriptions for the attenuation can be inaccurate. We have developed a method for implementing an exact solution to the radiation transport that can be easily combined with any independent emission model, such as the Astrophysical Plasma Emission Code (APEC) (Smith et al. 2001) that is widely used in fitting stellar X-ray spectra. This can be used to realistically model the low-resolution CCD spectra that are produced in large quantities by surveys of clusters and OB associations with *Chandra* and *XMM*-Newton (e.g., Wang et al. 2008). It can also be used to model grating spectra in detail, and provides a means of disentangling the wind absorption effects from the emission temperature effects that appear to both contribute to the recently discovered trend in the morphology of OB star spectra observed at high resolution with the *Chandra* gratings (Walborn et al. 2009).

2. RADIATION TRANSPORT MODEL

In this section, we derive an expression for the fraction of X-rays transmitted from a massive star wind as a function of the wavelength-dependent opacity and the wind density. We make assumptions similar to those made in Owocki & Cohen (2001): we model the wind as a two-component fluid, where a small fraction of the wind is heated to X-ray emitting temperatures ($T_{\rm X} \sim 1 - 10\,{\rm MK}$), while the bulk of the wind is composed of relatively cool material ($T_{\rm wind}/T_{\rm eff} \sim 0.5 - 1$) which can absorb the X-rays via the bound-free opacity of the moderately ionized metals. We also assume that the X-ray spectrum is the same over the the entire emitting volume; this is consistent with the finding of Cohen et al. (2006, 2010) in their detailed study of the emission line profiles of ζ Ori and ζ Pup that the onset radius of X-ray emission is roughly the same for all ions observed.

The observed X-ray emission at a given wavelength is

[1] Laboratory for High Energy Astrophysics, Code 662, NASA/Goddard Space Flight Center, Greenbelt, MD 20771;
[2] NASA Postdoctoral Fellow
[3] Department of Physics and Astronomy, Swarthmore College, Swarthmore, PA 19081
[4] IPN, Mexico City
[5] Department of Physics and Astronomy, University of Pittsburgh, 3941 O'Hara Street, Pittsburgh, PA 15260
[6] Department of Astronomy, University of Chicago, Chicao, IL 60637
[7] Bartol Research Institute, University of Delaware, Newark, Delaware 19716, USA
[8] Department of Geology and Astronomy, West Chester University of Pennsylvania, West Chester, Pennsylvania 19383, USA

given by

$$L_\lambda = 4\pi \int dV\, \eta_\lambda(r)\, e^{-\tau(r,\mu,\lambda)}\,, \tag{1}$$

where $\eta_\lambda(r)$ is the X-ray emissivity, and $\tau(r,\mu,\lambda)$ is the continuum optical depth of the dominant cool component along a ray from the emitting volume element to the observer.

The optical depth can be derived as in Owocki & Cohen (2001) for a smooth wind. It is given by the integral

$$\tau(p,z,\lambda) = \int_z^\infty dz'\, \kappa_\lambda\, \rho(r')\,. \tag{2}$$

Here p and z are ray coordinates, with impact parameter $p = \sqrt{1-\mu^2}\, r$ and distance along the ray $z = \mu\, r$. κ_λ is the atomic opacity of the wind, and $\rho(r)$ is the density of the wind. Using the continuity equation, $\rho(r) = \dot{M}/4\pi r^2 v(r)$, where $\dot{M}$ is the stellar mass loss rate, and defining the *characteristic wind optical depth*,

$$\tau_* \equiv \frac{\kappa_\lambda\, \dot{M}}{4\pi R_* v_\infty}\,, \tag{3}$$

we can write

$$\tau(p,z) = \tau_*\, t(p,z)\,, \tag{4}$$

where

$$t(p,z) \equiv \int_z^\infty \frac{R_* dz'}{r'^2 w(r')} \tag{5}$$

is an integral that depends purely on the ray geometry. Here R_* is the stellar radius, v_∞ is the wind terminal velocity, and $w(r) \equiv v(r)/v_\infty$ is the scaled wind velocity. Note that we have assumed that κ_λ is constant throughout the wind; we further discuss this assumption in § 3.

We take the velocity to follow a beta law: $v = v_\infty(1 - R_*/r)^\beta$. We also take $\beta = 1$ in this paper as a good approximation for many O star winds; however, evaluation for general values of β is not difficult.

The emissivity is assumed to scale with density squared, as in Owocki & Cohen (2001). Because we are interested in broadband X-ray transmission of the wind rather than detailed line profile shapes, we ignore the Doppler shift of the emitted X-rays and write

$$\eta_\lambda(r > R_0) = \eta_{\lambda,0} \frac{\rho^2(r)}{\rho_0^2}\,. \tag{6}$$

Here we assume that X-ray emission begins at a minimum radius R_0, with $\rho_0 = \rho(R_0)$ and $\eta_{\lambda,0} = \eta_\lambda(R_0)$. In this paper, we will assume that the X-ray filling factor is constant with radius; it is trivial to add a power-law radial dependence, as in OC01. Finally, we assume that X-ray emissivity follows the same radial distribution at all observable wavelengths.

The model described in the preceding paragraphs is illustrated in Figures 1 and 2. The model emissivity and transmission are visualized separately in Figure 1, and together in the left panel of Figure 2. The right panel of Figure 2 gives the net transmission for the exospheric approximation for comparison, which we will discuss at more length subsequently.

Using Eqs. 1-6, we can calculate the transmission of the wind as a function of τ_*. The transmission is simply

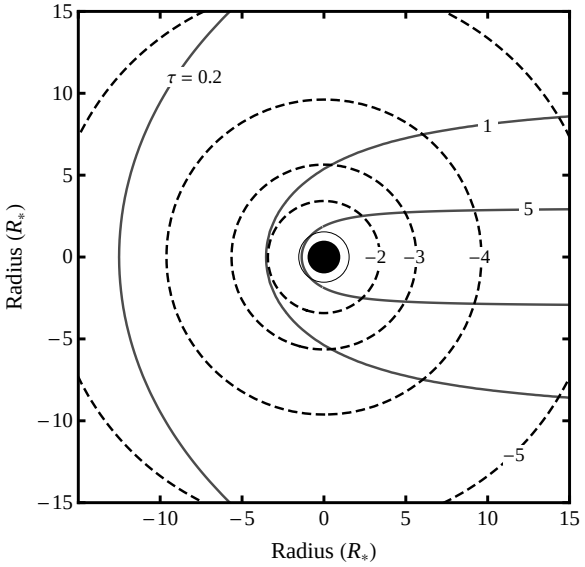

Figure 1. This diagram shows the X-ray emission and absorption properties of a model stellar wind. The observer is on the left. Contours of constant X-ray emissivity (proportional to density squared) are shown with dashed lines at intervals of an order of magnitude in differential emissivity. The absolute scale is normalized to the maximum emissivity at the onset radius of X-ray emission. Contours of constant continuum optical depth calculated for $\tau_* = 3$ are shown with solid lines.

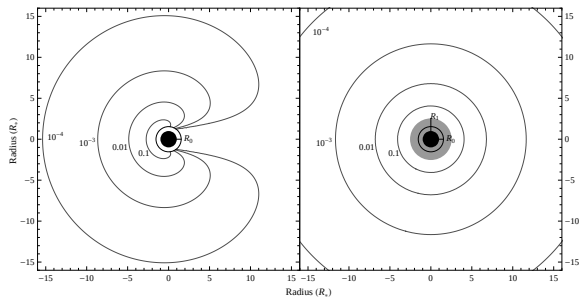

Figure 2. The left panel is the same as Figure 1, but plotting the renormalized product of emissivity times transmission, including occultation by the stellar core. The right panel shows the same plot in the exospheric approximation, where the grey zone is inside the radius of (radial) optical depth unity and thus does not contribute to the observed X-ray flux.

the observed flux (Eq. 1) divided by the unattenuated flux, which can be found by setting $\tau_* = 0$ in the same equation:

$$T(\tau_*) = \frac{\int dV\, \rho^2\, e^{-\tau}}{\int dV\, \rho^2}\,. \tag{7}$$

The numerator of this equation can most easily be evaluated by first numerically integrating the angular component of the integral for a shell at radius r to obtain the *angle averaged transmission*:

$$\overline{T}(r,\tau_*) = \frac{1}{2}\int_{\mu_*}^1 d\mu\, e^{-\tau_* t(r,\mu)}\,, \tag{8}$$

where

$$\mu_* = \sqrt{1 - \frac{R_*^2}{r^2}} \tag{9}$$

gives the μ coordinate of occultation by the the stellar core. Some X-rays are obscured by the stellar core even

when the wind is transparent:

$$\overline{T}_0(r) \equiv \overline{T}(r,0) = \frac{1}{2}(1-\mu_*)\,. \tag{10}$$

Integrating over shells at all radii, the net transmission is thus

$$T(\tau_*) = \frac{\int_{R_0}^{\infty} dr\, r^2\, \rho^2(r)\, \overline{T}(r,\tau_*)}{\int_{R_0}^{\infty} dr\, r^2\, \rho^2(r)}\,. \tag{11}$$

We can further evaluate this expression by substituting the continuity equation, and by defining the inverse radial coordinate $u \equiv R_*/r$:

$$T(\tau_*) = \frac{\int_0^{u_0} du\, w^{-2}(u) \overline{T}(u,\tau_*)}{\int_0^{u_0} du\, w^{-2}(u)}\,. \tag{12}$$

In Figure 3 we show $\bar{T}(u)$ for selected values of τ_*. Figure 4 we show $T(\tau_*)$ for our model, along with comparisons to two other absorption prescriptions: a simple intervening absorber, $T = e^{-\tau}$, appropriate for a coronal slab model, e.g. as implemented in the XSPEC models *wabs* or *tbabs*; and an exospheric approximation (e.g. Owocki & Cohen 1999), where $T = 0$ below the radius of optical depth unity, and $T = 1$ everywhere above it:

$$T_{\rm exo}(\tau_*) = \frac{\int_0^{u_1(\tau_*)} du\, w^{-2}(u)}{\int_0^{u_0} du\, w^{-2}(u)}\,. \tag{13}$$

The inverse radial coordinate of optical depth unity is given by evaluating the optical depth integral (Eq. 5) along a radial ray ($p = 0$, $z = r$), with the result

$$u_1(\tau_*) = 1 - e^{-1/\tau_*}\,, \tag{14}$$

for $\beta = 1$. Note that in both Figures 3 and 4 we have used $\beta = 1$ and $R_0 = 1.5R_*$. We stress that Eq. 13 is simply the consequence of using a step function for the angle-averaged transmission $\overline{T}$ in Eq. 12, rather than the more realistic expression given in Eq. 8.

Thus, the transmission of our model falls off much more gradually than $e^{-\tau}$, but it is also more accurate than the exospheric approximation, especially at moderate optical depth. Note that the angle averaged transmission curves plotted in Figure 3 are the essential difference between the radiation transport model of *windtabs* and that of the exospheric model.

We note that it would be simple to generalize the radiation transport model described in this section to include porosity by introducing an appropriate definition of effective opacity, as in Oskinova et al. (2006) or Owocki & Cohen (2006). However, a specific implementation of this and discussion of its consequences is beyond the scope of this paper.

Finally, to find the transmission of a stellar wind as a function of wavelength, we must first find τ_* as a function of wavelength; we can then combine this with Eq. 12 to evaluate the transmission for a specific set of wind properties (see Eq. 3 for the explicit dependence of τ_* on κ_λ). The wavelength dependence of τ_* is introduced through the opacity. It is thus useful to write

$$\tau_*(\lambda) = \kappa_\lambda \Sigma_*\,, \tag{15}$$

where

$$\Sigma_* \equiv \frac{\dot{M}}{4\pi R_* v_\infty} \tag{16}$$

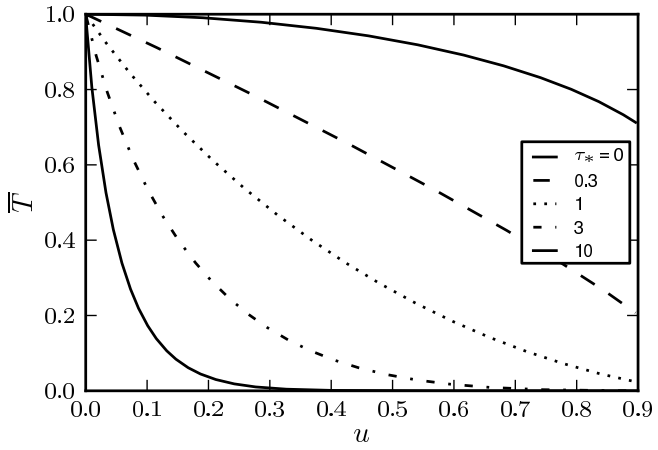

Figure 3. Angle averaged transmission $\overline{T}$ as a function of shell inverse radial coordinate $u = R_*/r$, with different curves for different characteristic wind optical depths τ_*. Note that the transmission is less than unity even for $\tau_* = 0$ due to occultation by the stellar core. The equivalent plot in the exospheric approximation would be a step function at u_1, the inverse radial coordinate of optical depth unity.

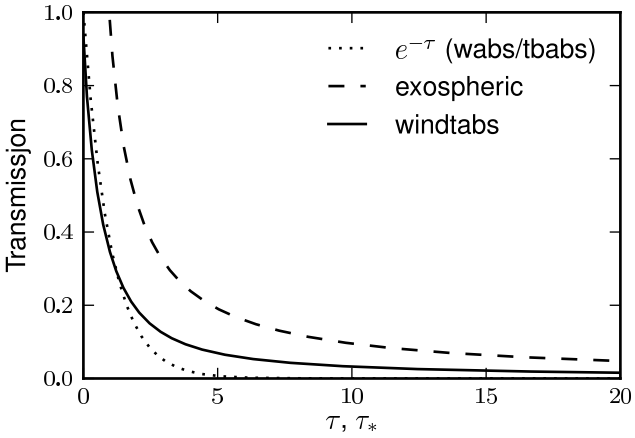

Figure 4. Comparison of transmission of three different models: coronal slab ($e^{-\tau}$), exospheric, and more realistic wind model (*windtabs*). The fixed parameters are $\beta = 1$, $R_0 = 1.5$.

is the *characteristic mass column density* of the wind (in $\mathrm{g\,cm^{-2}}$). The determination of the opacity is the subject of § 3.

3. OPACITY MODEL

The continuum opacity of a stellar wind in the X-ray band can be calculated by summing the contributions of each constituent species. Thus, we must know the elemental abundances, ionization fractions, and the atomic opacities. Of these three, the opacities are well known to sufficient accuracy (e.g. Verner & Yakovlev 1995); the ionization balance may contribute some uncertainty in the calculation of the opacity, but is usually not the dominant contribution; and uncertainties in the elemental abundances are typically the most important.

The opacity due to photoionization of a given shell of any individual species scales approximately as $\kappa_i(E >$

$E_{\rm th}) \propto E^{-3}$ above the threshold energy $E_{\rm th}$ of the shell. Because multiple species are usually important for the X-ray opacity of astrophysical gas, the run of opacity with wavelength has a characteristic sawtooth shape, with individul teeth at the ionization threshold energies of dominant ionization stages of abundant elements.

O star winds are photoionized, with H and He fully stripped, and most other elements mainly in charge states +3 and +4; thus, the opacity of stellar winds in the range $1\,\text{Å} < \lambda < 40\,\text{Å}$ is dominated by K-shell absorption in C, N, and O, since they are the most abundant elements.

The opacity of adjacent ionization stages of the same element are usually comparable, with the exception that the photoionization threshold energy is shifted. As long as the precise threshold energies are not important in spectral modeling, the effect of a moderate shift in ionization balance on the opacity is relatively minor; however, the difference in threshold energies between neutral material and O star winds is significant.

Therefore, while it is important to use an appropriate model for the ionization of an O star wind, it is sufficient for many applications to use a single approximate ionization balance to model all O star winds. This is true even though the ionization balance can vary to some extent with radius, and also is different in different O stars.

If it is desired to model the opacity of a particular star, it is possible to construct a detailed model opacity for a stellar wind by using the output of a radiative transfer model such as CMFGEN (Hillier et al. 1993; Hillier & Miller 1998; Cohen et al. 2010, Zsargo et al., in preparation).

To illustrate the importance of various assumptions in opacity modeling, in Figures 5 and 6 we compare a number of model opacities. Figure 5 compares neutral interstellar medium opacity and a simple model for the opacity of a stellar wind. Both assume solar abundances (Asplund et al. 2009). In the wind model we assume an ionization balance with hydrogen and helium fully stripped, oxygen and nitrogen in the +3 charge state, and all other elements in the +4 charge state. The wind opacity is much lower, especially at long wavelengths, mainly due to the ionization of hydrogen and helium. The shift in ionization threshold energies is also clear.

Figure 6 shows the same simple model described in the previous paragraph; as well as a more realistic model particular to ζ Pup, using non-solar abundances specific to the star, and generated by calculating the opacity at $\sim 2R_*$ from a detailed CMFGEN model (Zsargó et al. 2008, Bouret et al., in preparation; Zsargo et al., in preparation); and finally, a simplified version of the CMFGEN model, using the same abundances, but the simplified ionization structure of the solar abundance wind opacity model. The fact that the realistic CMFGEN ζ Pup model and the simplified version are so similar indicates that a simple ionization balance is typically adequate to describe wind opacity in many cases, as long as it is relatively accurate. On the other hand, the difference between the ζ Pup models and the solar abundance model shows that the opacity model depends strongly on the abundances of the most common elements other than H and He (typically C, N, and O). Note that the Bouret et al. abundances for ζ Pup are non only non-solar in the ratio of CNO, but also are sub-solar, which accounts for the lower opacity of the ζ Pup models at short wavelengths compared to the solar abundance model.

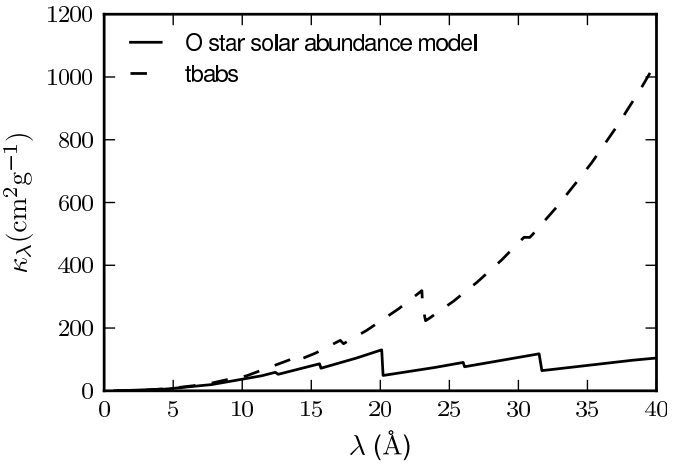

Figure 5. Comparison of a neutral interstellar absorption model (including dust grains), *tbabs* (Wilms et al. 2000); and an O star wind model with an assumed simple ionization structure. Both use solar abundances (Asplund et al. 2009). Note that even below the O^3+ edge near 20 Å, the realistic wind opacity model is still about 40% lower than the ISM model, mainly due to the ionization of H and He in the wind model.

We have made one important simplification in our modeling: in Eq. 4, and throughout this section, we have assumed that the opacity is independent of radius. As we have shown in Figure 6, moderate changes in wind ionization do not strongly affect the opacity, so in most cases this is a justified assumption. The important exception is the ionization of helium; in sufficiently dense winds, He^{++} may recombine to He^+ in the outer part of the wind, which greatly increases the opacity, especially at long wavelengths (Hillier et al. 1993). As long as the change in ionization occurs sufficiently far out in the wind, geometrical effects as described in § 2 are not important, and the absorption due to He^+ can be treated as an additional slab between the X-ray emitting regions and the observer, i.e. using $T = e^{-\tau}$.

4. MODEL IMPLEMENTATION

The numerical evaluation of Eq. 12 is not prohibitively expensive, but it is typically not fast enough to allow its use in an automated spectral fitting routine, such as that in XSPEC (Arnaud 1996) or ISIS (Houck & Denicola 2000). It is thus preferable to compute the transmission on a grid in τ_* for a given set of wind parameters.

Given a tabulation of the model wind opacity, as described in § 3, in addition to the tabulation of $T(\tau_*)$, one may then calculate the transmission as a function of wavelength, $T(\lambda)$, with only one free parameter, the characteristic wind mass column density Σ_*. This parameter is analagous to the neutral hydrogen column density in a slab absorption model such as the XSPEC *wabs* model.

We have implemented this as a local model for XSPEC 12. $T(\tau_*)$ may be calculated for a given set of parameters (i.e. β, R_0), with the results stored in a FITS table. The model opacity must also be supplied as a FITS file; different model opacities may be swapped in at run time. The calculation of $T(\tau_*)$ is controlled by a simple python

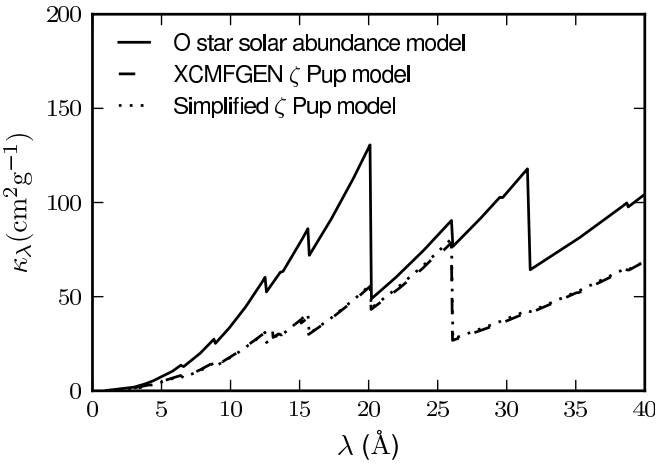

Figure 6. Comparison of three different model O star wind opacities: the solar abundance O star wind model shown in Fig 5 (solid); an XCMFGEN model appropriate for ζ Pup (dashed) using the abundances of Bouret et al. (in preparation); and a simplified version of this XCMFGEN model (dotted) where the ionization balance is the same as in the solar abundance model. Note that the Bouret et al. abundances for ζ Pup are subsolar as well as having altered CNO abundance ratios.

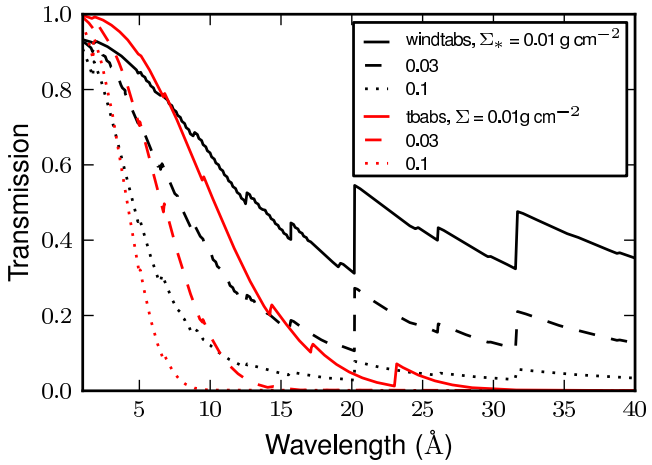

Figure 7. Transmission as a function of wavelength for ionized wind absorption model (*windtabs*, black) and for neutral slab absorption (*tbabs*, red). Three values of absorbing column are given; for *windtabs*, the degree of absorption is specified by the characteristic mass column density Σ_*, while for *tbabs* it is given simply by the mass column Σ.

script, and computation of a table for a given set of parameters can be accomplished in several seconds on a modern workstation.

The model transmission is then calculated as a function of energy or wavelength, using the supplied FITS tables and the one free model parameter, Σ_*. This parameter is in analogy with the neutral hydrogen column density N_H typically used as the free parameter for interstellar absorption models.

Note that there are additional implicit model parameters that go into the tabulation of $T(\tau_*)$: the velocity law power index β, and the onset radius of X-ray emission, R_0. These parameters may be varied by computing additional table models and substituting the FITS tables used by the XSPEC local model. However, the absorption model is not very sensitive to these parameters over the range typically inferred for winds of massive stars.

Note that the elemental abundances, which enter into the transmission through their effect on the opacity, cannot be varied as fit parameters in our model. This is a choice we have made in the model implementation, both for computational ease and simplicity of user interface, and because there is not enough information in X-ray spectra alone to break degeneracies between elemental abundances, X-ray emission temperature distribution, and wind column density. Abundances should be inferred by other means, and can be used to compute a new opacity table for a given star.

In Figure 7 we give the model transmission for *windtabs* using three different values of Σ_*. For comparison, we also give the transmission for the neutral absorption model *tbabs* for comparable mass column densities Σ. Note that Σ refers simply to a slab mass column density, while Σ_* refers to a *characteristic* mass column density in the context of a stellar wind (see Eq 16).

5. DISCUSSION

The exact method we have presented here for modeling the emergent X-ray flux from a spatially distributed source embedded within a partially optically thick wind is crucial for analyzing and interpreting the X-ray emission observed from O stars. Compared to the exponential, neutral slab absorption (excess over ISM) model that is usually employed, the *windtabs* model accurately reproduces the much more gradual decrease in transmission with increasing wind column density and opacity. Using an accurate wind transmission prescription is important for attempts to understand the broadband spectral energy distributions of individual stars; compare the transmission as a function of wavelength for any one black curve in Figure 7 to the corresponding curve in red. And it is also relevant for understanding trends in X-ray properties within a sample of O stars with winds having a range of optical thicknesses; compare the trend in transmission over any wavelength range in Figure 7 as one looks to denser and denser winds: solid to dashed to dotted black curves show a gradual decrease in transmission with characteristic optical depth τ_*, or column density, while the decrease in transmission among the corresponding red curves is much more drastic.

As Figure 4 shows, once a wind becomes optically thick, the exponential absorption model will significantly overestimate the amount of X-ray attenuation, leading to underestimates of the characteristic wind column density and associated mass-loss rate. And because the opacity of the bulk wind is a relatively strong function of wavelength, the inaccuracy of the exponential transmission model will also lead to errors in the broadband spectral energy distribution of a model applied to a single object, leading to misinterpretations of the associated emission model components. This appears to be the case in the X-ray abundance study in Zhekov & Palla (2007), where the authors rely on excess exponential, neutral ISM absorption to account for the assumed wind attenuation, and find an unphysical correlation between their derived elemental abundances and the wavelength of the emission lines used for the abundance determinations.

The exospheric model, which incorporates the more gradual decrease in transmission via an inherently spher-

ically symmetric, simplified treatment of the radiation transport, is more accurate than the slab model with its exponential attenuation. However, the exospheric model leads to an overestimate of the transmission compared to the more accurate windtabs model. This is especially true for moderate optical depths; indeed, for characteristc optical depths τ_* less than unity, the exospheric model predicts no attenuation at all, and will overestimate the true transmission by a factor of several.

It has long been noted that the exponential attenuation treatment is not well suited to modeling OB star X-rays. Cohen et al. (1996) showed that an exospheric treatment, rather than an exponential treatment, is important for understanding the observed EUV and soft X-ray emission from the early B giant, ϵ CMa. The exospheric approximation was used by Owocki & Cohen (1999) to model the effect of wind attenuation of X-rays in order to explain the observed $L_x/L_{bol} \sim 10^{-7}$ relationship and its breakdown in the early B spectral range where hot star winds become optically thin to X-rays. An exospheric treatment was also used by Oskinova et al. (2001) to analyze the variability of X-rays from optically thick WR winds. And the exospheric framework forms the basis for the "optical depth unity" relationship for X-rays in O stars, where the forbidden-to-intercombination line ratios of helium-like ions are claimed to imply formation radii that track the optical depth unity radius as a function of X-ray wavelength (Waldron & Cassinelli 2007). However, if treatments such as these are to be used to analyze real data with a high degree of accuracy, then a more realistic treatment of X-ray radiation transport through the wind must be used; one that takes the inherently non-spherically symmetric nature of the problem into account. This is especially true when the location of the X-ray emission that is emergent from the wind is important, as with the interpretation of f/i ratios. As Figure 2 shows, the relative contribution toward the emergent X-ray flux from different wind regions is grossly misrepresented in the exospheric approach. In any case, to assess the implications of low f/i ratios, a spatially distributed emission model should be used along with an accurate treatment of the radiation transport, as in *windtabs*.

The *windtabs* model we have introduced here is not only more accurate in terms of the radiation transport, but it has two additional advantages that recommend its adoption for routine X-ray data analysis and modeling of O stars. First, it is easy to use and has only a single free parameter, the characteristic mass column density Σ_*, from which a mass-loss rate can be readily extracted. And second, it incorporates a default wind opacity model that is significantly different from, and much more accurate than, the neutral ISM opacity models that are usually used. Additionally, alternate user-calculated opacity models are easy to incorporate.

One application of *windtabs* to the interpretation of X-ray spectral data is for the analysis of the X-ray spectral hardness trend vs. optical spectral subtype recently noted in *Chandra* grating spectra by Walborn et al. (2009). Claimed to be an ionization or temperature trend inherent to the production of X-rays, clearly the broadband trend is affected by differential wind absorption of soft X-rays. A detailed analysis is in preparation,

Table 1
Adopted stellar parameters

Star	Type[a]	$N_{\rm H}$[b]	Σ_*[c]
HD 150136	O3.5 I	0.36	0.073
ζ Pup	O4 I	0.01	0.160
ξ Per	O7.5 III	0.115	0.017
τ CMa	O9 II	0.056	0.013
δ Ori	O9.5 II	0.015	0.011
ζ Ori	O9.7 I	0.03	0.019
ϵ Ori	B0 I	0.03	0.020

[a] (Ref to walborn)
[b] Interstellar medium column density (10^{22}cm^{-2})
[c] Characteristic wind mass column density (g cm^{-2})

but here we show a single suite of models in which the only variable parameter is the characteristic wind column density, Σ_*. A single emission model, combined with *windtabs* attenuation, reproduces the observed broadband trend quite well.

We reproduce the trend noted by Walborn et al. (2009) in Figure 8, where the data for seven O giants and supergiants are shown in the left-hand column, with the earliest spectral subtype (O3.5) on the top, and the latest (B0) on the bottom. The later spectral subtypes clearly have more soft X-ray emission, although the earlier subtypes still have non-negligible long-wavelength ($\lambda \gtrsim 15$ Å) emission. In the middle column we show a four-temperature APEC (Smith et al. 2001) thermal equilibrium emission model; we have chosen $kT = 0.1$, 0.2, 0.4, and 0.8 keV; the first three components having equal emission measures and the hottest one having half the emission measure of the others. The same APEC model is used for all seven stars (with variable overall normalization) and is multiplied by a *windtabs* model and a *tbabs* model (for neutral ISM attenuation). The column density of the *tbabs* model is fixed at the interstellar value taken from Fruscione et al. (1994), with the exception of HD 150136, for which we inferred the ISM column density from E(B-V) [**refs**]. The characteristic mass column density Σ_* in *windtabs* is fixed at a value computed from the "cooking formula" theoretical mass-loss rate computed by Vink et al. (2001), using the measured terminal velocity of Haser et al. (1998) and the modeled radii of Martins et al. (2005). The standard solar abundance wind opacity model (solid line in Figure 6) was used in windtabs, and the APEC model abundances were set to solar. There are no free parameters in these models, and the temperature distribution has not even been significantly optimized to match the data. The adopted parameters are listed in Table 1.

As the middle column of Figure 8 shows, the simple, universal emission model reproduces the broadband trend very well. Trends in individual line ratios generally cannot be reproduced only by accounting for the varying attenuation, as pointed out by Walborn et al. (2009), but note that the Ne IX (13.5 Å) to Ne X (12.1 Å) ratio does indeed vary due only to differential attenuation among the earliest spectral subtypes. The right-hand column in Figure 8 shows the same emission and ISM attenuation models as in the middle column, but with excess exponential (neutral ISM) attenuation accounting

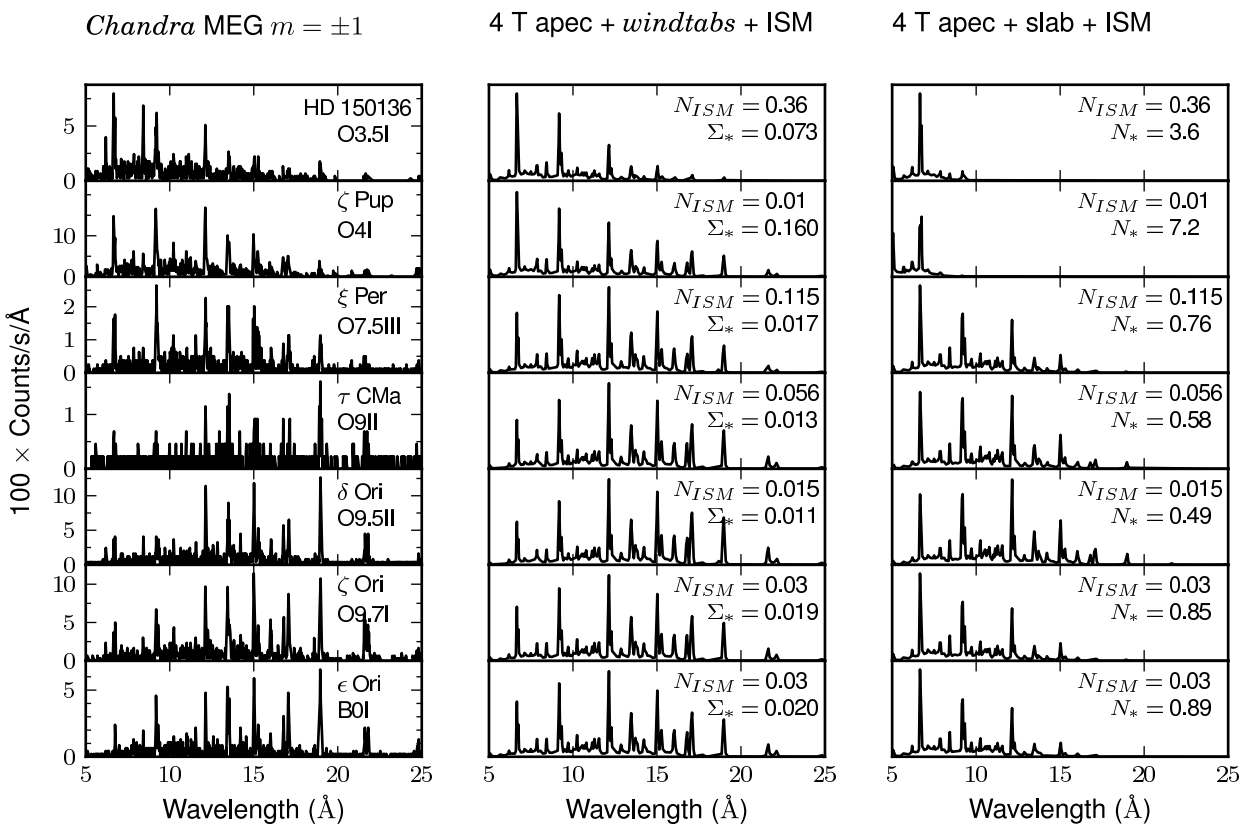

Figure 8. Left column: a sequence of *Chandra* spectra of O giants and supergiants from Walborn et al. (2009); middle column: multi-temperature thermal emission model with *windtabs* wind absorption model; right column: same model as middle column, but with *tbabs* neutral slab absorption model.

for the wind absorption, again according to the wind column densities expected from the adopted mass-loss rates, radii, and terminal velocities. The exponential attenuation trend seen in the right-hand column is too strong for the earliest spectral subtypes and too weak for the latest ones, where the different ISM column densities actually dominate the trend.

The contrast between the windtabs and exponential models is quite stark, and indicates that the more realistic models should generally be used when analyzing X-ray spectra, both high-resolution and broadband. It is also impressive how much of the observed spectral hardness trend is explained by wind attenuation, in the context of a realistic model. Not only do quantitative analyses of the suggested line ratio trends have to be evaluated, but a global spectral modeling that allows for both emission temperature variations and wind attenuation variations should be undertaken in order to disentangle the relative contributions of trends in emission and absorption to the overall, observed trend in the spectral energy distributions.

6. CONCLUSIONS

We have presented an exact solution to the radiation transport of X-rays through a spherically symmetric, partially optically thick O star wind, and shown that it differs significantly from the commonly used slab absorption and exospheric models. Specifically, the transmission falls off much more gradually as a function of fiducial optical depth in the windtabs model as compared to the exponential model, leading to more accurate assessments of wind column densities and mass-loss rates from fitting X-ray spectra. As one example of the utility of windtabs, we have shown that when this more accurate model is employed, differential wind absorption can explain most of the observed trend in OB star X-ray spectral hardness with spectral subtype, and even may explain some of the line ratio trend.

The windtabs model has been implemented as a custom model in XSPEC, and is as easy to use as the various ISM absorption models, having only one free parameter. In addition to the significantly improved accuracy of the radiation transport, windtabs has several other advantages. It incorporates a default opacity model much more appropriate to stellar winds than the neutral element opacity model used in ISM attenuation codes. Users can easily substitute their own custom-computed opacity models. And the fitted mass column density parameter for windtabs easily allows for the user to extract a mass-loss rate from their fitting of X-ray spectra of OB stars.

MAL is supported by an appointment to the NASA Postdoctoral Program at Goddard Space Flight Cen-

ter, administered by Oak Ridge Associated Universities through a contract with NASA.

REFERENCES

Arnaud, K. A. 1996, in Astronomical Society of the Pacific Conference Series, Vol. 101, Astronomical Data Analysis Software and Systems V, ed. G. H. Jacoby & J. Barnes, 17–+
Asplund, M., Grevesse, N., Sauval, A. J., & Scott, P. 2009, ARA&A, 47, 481
Cassinelli, J. P. & Olson, G. L. 1979, ApJ, 229, 304
Cassinelli, J. P. & Swank, J. H. 1983, ApJ, 271, 681
Cohen, D. H., Cooper, R. G., MacFarlane, J. J., Owocki, S. P., Cassinelli, J. P., & Wang, P. 1996, ApJ, 460, 506
Cohen, D. H., Leutenegger, M. A., Grizzard, K. T., Reed, C. L., Kramer, R. H., & Owocki, S. P. 2006, MNRAS, 368, 1905
Cohen, D. H., Leutenegger, M. A., Wollman, E. E., Zsargo, J., Hillier, D. J., Townsend, R. H. D., & Owocki, S. P. 2010, submitted to MNRAS, http://astro.swarthmore.edu/zPupCohen.pdf
Fruscione, A., Hawkins, I., Jelinsky, P., & Wiercigroch, A. 1994, ApJS, 94, 127
Haser, S. M., Pauldrach, A. W. A., Lennon, D. J., Kudritzki, R.-P., Lennon, M., Puls, J., & Voels, S. A. 1998, A&A, 330, 285
Hillier, D. J., Kudritzki, R. P., Pauldrach, A. W., Baade, D., Cassinelli, J. P., Puls, J., & Schmitt, J. H. M. M. 1993, A&A, 276, 117
Hillier, D. J. & Miller, D. L. 1998, ApJ, 496, 407
Houck, J. C. & Denicola, L. A. 2000, in Astronomical Society of the Pacific Conference Series, Vol. 216, Astronomical Data Analysis Software and Systems IX, ed. N. Manset, C. Veillet, & D. Crabtree, 591–+
Kahn, S. M., Leutenegger, M. A., Cottam, J., Rauw, G., Vreux, J.-M., den Boggende, A. J. F., Mewe, R., & Güdel, M. 2001, A&A, 365, L312
MacFarlane, J. J., Cohen, D. H., & Wang, P. 1994, ApJ, 437, 351
Martins, F., Schaerer, D., & Hillier, D. J. 2005, A&A, 436, 1049
Oskinova, L. M., Feldmeier, A., & Hamann, W.-R. 2006, MNRAS, 372, 313
Oskinova, L. M., Ignace, R., Brown, J. C., & Cassinelli, J. P. 2001, A&A, 373, 1009
Owocki, S. P. & Cohen, D. H. 1999, ApJ, 520, 833
—. 2001, ApJ, 559, 1108
—. 2006, ApJ, 648, 565
Smith, R. K., Brickhouse, N. S., Liedahl, D. A., & Raymond, J. C. 2001, ApJ, 556, L91
Verner, D. A. & Yakovlev, D. G. 1995, A&AS, 109, 125
Vink, J. S., de Koter, A., & Lamers, H. J. G. L. M. 2001, A&A, 369, 574
Walborn, N. R., Nichols, J. S., & Waldron, W. L. 2009, ApJ, 703, 633
Waldron, W. L. & Cassinelli, J. P. 2007, ApJ, 668, 456
Wang, J., Townsley, L. K., Feigelson, E. D., Broos, P. S., Getman, K. V., Román-Zúñiga, C. G., & Lada, E. 2008, ApJ, 675, 464
Wilms, J., Allen, A., & McCray, R. 2000, ApJ, 542, 914
Zhekov, S. A. & Palla, F. 2007, MNRAS, 382, 1124
Zsargó, J., Hillier, D. J., Bouret, J., Lanz, T., Leutenegger, M. A., & Cohen, D. H. 2008, ApJ, 685, L149